Biomaterials and Biomechanics in Bioengineering, *Vol. 3, No. 1 (2016) 1-14*
DOI: http://dx.doi.org/10.12989/bme.2016.3.1.001

Finite element modeling of manufacturing irregularities of porous materials

Fernando J. Quevedo González* and Natalia Nuño

Laboratoire de recherche en Imagerie et Orthopédie (LIO), Département de Génie de la Production Automatisée, École de Technologie Supérieure, 1100 rue Notre-Dame Ouest, H3C 1K3 Montréal, Canada

(Received June 30, 2015, Revised September 10, 2015, Accepted October 14, 2015)

Abstract. Well-ordered porous materials are very promising in orthopedics since they allow tailoring the mechanical properties. Finite element (FE) analysis is commonly used to evaluate the mechanical behavior of well-ordered porous materials. However, FE results generally differ importantly from experimental data. In the present article, three types of manufacturing irregularities were characterized on an additive manufactured porous titanium sample having a simple cubic unit-cell: strut diameter variation, strut inclination and fractured struts. These were included in a beam FE model. Results were compared with experimental data in terms of the apparent elastic modulus (Eap) and apparent yield strength (SY,ap). The combination of manufacturing irregularities that yielded the closest results to experimental data was determined. The idealized FE model resulted in an Eap one order of magnitude larger than experimental data and a SY,ap almost twice the experimental values. The strut inclination and fractured struts showed the strongest effects on Eap and SY,ap, respectively. Combining the three manufacturing irregularities produced the closest results to experimental data. The model also performed well when applied to samples having different structural dimensions. We recommend including the three proposed manufacturing irregularities in the FE models to predict the mechanical behavior of such porous structures.

Keywords: additive manufacturing; electron beam melting; porous materials; finite element; manufacturing irregularities; mechanical properties

1. Introduction

Well-ordered porous metallic materials, also known as lattice materials, are formed by an arrangement of struts at the mesoscale. These structured materials are very promising in aerospace industry (Heo *et al*. 2013, Spadoni and Ruzzene 2007), heat transfer (Kumar *et al*. 2009, Maloney *et al*. 2012) or shock absorption (Harrigan *et al*. 2010), but specially in orthopedic applications (Arabnejad and Pasini 2013, Parthasarathy *et al*. 2011). The mechanical properties of these materials are dependent on the mesoscale shape (i.e., diamond, simple cubic, etc.) and dimensions (strut and pore diameters, porosity, etc.), thus can be tailored for specific needs (Luxner *et al*. 2005). Moreover, mechanical properties can be varied throughout a piece, making possible to

*Corresponding author, Ph.D. Student, E-mail: fernandojquevedo@gmail.com
[a]Professor, E-mail: natalia.nuno@etsmtl.ca

http://www.techno-press.org/?journal=bme&subpage=7 ISSN: 2465-9835 (Print), 2465-9959 (Online)

produce “functionally graded implants” that reduce stress shielding and interfacial failure risk (Arabnejad and Pasini 2012, Kuiper and Huiskes 1997, Fraldi *et al.* 2010).

Finite element (FE) modeling is a powerful tool to these design lattice materials, since overall (at the macroscale) and local (at the mesoscale) mechanical behaviors can be obtained with the required level of detail. However, the mechanical behavior (in terms of the apparent elastic modulus E_{ap}) predicted with FE models generally differ importantly from experimental data, especially in the case of metallic lattice materials. For instance, for well-ordered porous titanium material with simple cubic (SC) unit-cell produced by Electron Beam Melting (EBM), Parthasarathy *et al.* (2011) predicted as much as 10 times stiffer response with FE models (E_{ap} between 20 and 30 GPa) than experimental data (E_{ap} from 2.13 to 2.92 GPa) for porosities ranging from approximately 51% to 70%.

For other unit-cell geometries at the mesoscale, these differences are smaller. For instance, for body centered cubic (BCC) unit-cell, Smith *et al.* (2013) found around 15% difference between numerical and experimental values of E_{ap}. For diamond (D) unit-cell geometry, Ahmadi *et al.* (2014) reported 15% difference and Herrera *et al.* (2014) an average of 27.5%. For an optimized unit-cell, Barbas *et al.* (2012) found a maximum difference of around 25% between FE and experimental E_{ap}.

The discrepancies between computational and experimental results may be caused by the manufacturing irregularities present on the physical samples, but that are usually not simulated in the FE models (Campoli *et al.* 2013). In addition, most studies consider only perfectly elastic material, instead of an elastic-plastic behavior which also contributes to enlarge the differences. In this way, some parametric studies exist about the relationship between the irregularities and the mechanical behavior of well-ordered porous materials (Chen *et al.* 1999, Zhu *et al.* 2001, Adjari *et al.* 2008, Alkhader and Vural 2008, Luxner *et al.* 2009), showing the influence of irregularities in the mechanical response.

However, very few authors have compared FE results for well-ordered porous materials including irregularities with experimental data. Campoli *et al.* (2013) considered the effect of strut diameter variation and material micro-porosities at the fused solid scale of titanium porous material, with results that were closer to experimental data. Hazlehurst *et al.* (2013) assumed that 50% of the elements of a continuum FE model of CoCrMo had reduced stiffness, obtaining a stiffness decrease of around 66% compared to an idealized model. Karamooz Ravari and Kadkhodaei (2015) obtained the equivalent material properties of an irregular strut of 316L stainless steel and applied them to an idealized beam FE model of a BCC unit-cell, resulting in an E_{ap} that was approximately 91% of the experimental values. However, except from Campoli *et al.* (2013) (who directly used measured values for the strut diameter variation), in the aforementioned studies, the E_{ap} decrease from the FE model was not obtained by the direct implementation of manufacturing irregularities measured on physical samples.

Therefore, the aim of this paper is to develop a simple approach to include the geometrical irregularities in a FE model based on observations to predict the mechanical behavior of well-ordered porous metallic materials. These geometrical irregularities are inherent to rapid manufacturing process of these materials. The objectives were to determine these irregularities directly from measurements of a physical sample made by EBM, and to include them in a beam FE model. To verify the validity of the proposed FE model, numerical results were compared to experimental data in terms of the apparent elastic modulus under compression (E_{ap}) and the apparent yield strength ($S_{Y,ap}$).

2. Materials and methods

2.1 Experimental data

Fabrication and mechanical testing were done at the Biomechanics Institute of Valencia (IBV, Spain). The most important details of the experimental procedure are depicted below. More details may be found in (Petrović *et al.* 2012).

The unit-cell and the macroscopic sample used by (Petrović *et al.* 2012) are shown in Fig. 1. At the mesoscale, simple cubic unit-cell with cylindrical struts was chosen (Fig. 1(a)). At the macroscale, samples had cubic shape and 10 unit-cells by side (Fig. 1(b)).

Three different sample sets with 5 samples per set (15 samples in total) of well-ordered Ti6Al4V porous material were fabricated by Electron Beam Melting (EBM). Design and measured diameters of struts (ϕ_S) and pores (ϕ_P) are shown in Table 1. Samples are referred to as "S" followed by the strut diameter, and "P" followed by the pore diameter (i.e., S450P700, for ϕ_S=450 μm ϕ_P=700 μm). Sample marked in bold (S450P700), is used for further characterization of the other manufacturing irregularities.

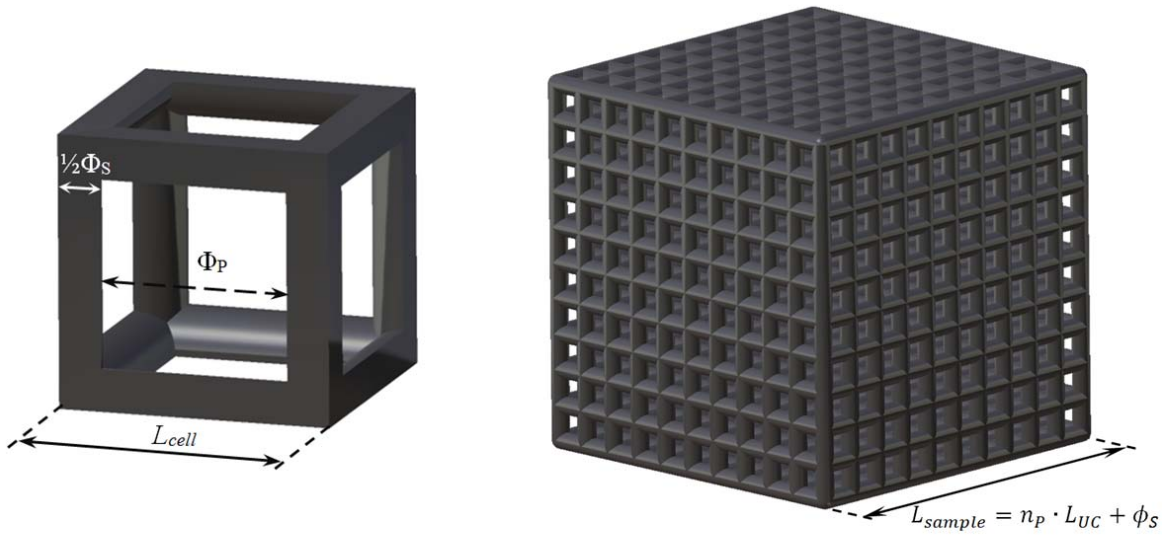

Fig. 1 (a) Cubic unit-cell pore geometry and main parameters and (b) 10-pore sample model generated by periodic repetitions of the unit-cell

Table 1 Design and experimental strut and pore sizes, from Petrovic *et al.* (2012)

Sample set	Design values		Measured values	
	$\phi_S(\mu\text{m})$	$\Phi_P(\mu\text{m})$	$\phi_S(\mu\text{m})$	$\Phi_P(\mu\text{m})$
S450P600	450	600	666	376
S450P700	**450**	**700**	**648**	**504**
S450P800	450	800	577	681

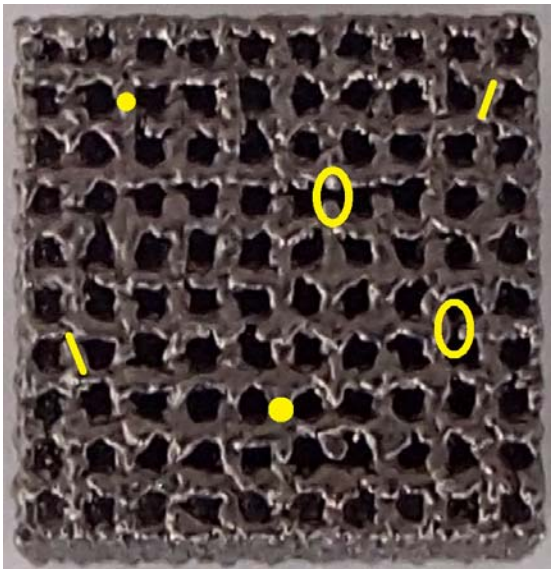

Fig. 2 Different types of geometrical manufacturing irregularities: strut diameter variation (solid points), strut inclination (straight lines) and fractured struts (empty circles)

2.2 FE modeling

Three types of geometrical irregularities due to the manufacturing process of the porous materials were identified at the mesoscale (Fig. 2): strut diameter variation; strut inclination; and fractured (or nearly fractured) struts. These irregularities were implemented in the FE model by altering an idealized model (without manufacturing irregularities). In total, 8 different FE models were created and simulated in ANSYS v14.5: i) the idealized model, ii) three models including the manufacturing irregularities separately, iii) four models including the possible combinations of manufacturing irregularities.

Material was modeled as bilinear elastic-plastic, based on Ti6Al4V-ELI data provided by the powder manufacturer (ARCAM AB.). An elastic modulus of E=120 GPa, a Poisson's ratio of ν=0.3, and a hardening modulus of K=1.4 GPa were used. Struts were modeled as in (Quevedo González and Nuño 2015), using straight lines and meshed with 3-node Timoshenko beam elements with circular cross-section and quadratic displacement behavior, which allow modeling moderately thick struts. A mesh sensitivity analysis showed that at least 2 elements (sharing a common node) were needed to mesh each strut. This resulted in 7260 elements for the idealized model.

Rigid surfaces (top and bottom) were used to simulate the experimental load application. Bonded contact (i.e., no sliding permitted) was considered, and pure Lagrange multiplier method was used. The bottom surface was fixed in all directions. A vertical displacement (i.e., normal to the surface) of 1.2 mm, similar to the one observed experimentally, was applied to the top surface.

2.2.1 Characterization and implementation of manufacturing irregularities in the FE model

A non-tested sample from the set S450P700 (ϕ_S=450 μm; ϕ_P=700 μm) was used. The three manufacturing irregularities and their implementation in the FE model are described below.

Strut diameter variation

The strut diameter was assumed to vary according to a normal distribution. The mean strut diameter for each sample set (μ_D) was taken as measured in the previous study of Petrović *et al.* (2012). Values are shown in Table 1. The maximum strut diameter variations were defined based on the maximum powder size, being of 100 μm, as schematized in Fig. 3: the maximum diameter is obtained when 2 powder particles are attached to the strut, whereas the minimum strut diameter is generated when 2 particle powders are not present. Therefore, a maximum diameter variation equal to 2 times the maximum powder size was assumed (i.e., μ_D±200 μm).

For the FE simulations, 9 circular beam cross-sections were created in ANSYS. Each cross-section accounted for diameters within ±25 μm (50 μm span) around its diameter value (Fig. 4). Each strut was then assigned with a random diameter value (ϕ_{rand}), issued from a normal distribution with a standard deviation of σ=75 μm (225/3 μm), chosen so that 99.8% of the values fell within μ_D±225 μm. Each assigned diameter was converted to the section number (S_n, from 1 to 9), according to Eq. (1).

$$Sn = \frac{\varphi_{rand} - \varphi_{\min}}{50} + 1 = \frac{\varphi_{rand} - (\mu_D - 3 \cdot \sigma)}{50} + 1 \tag{1}$$

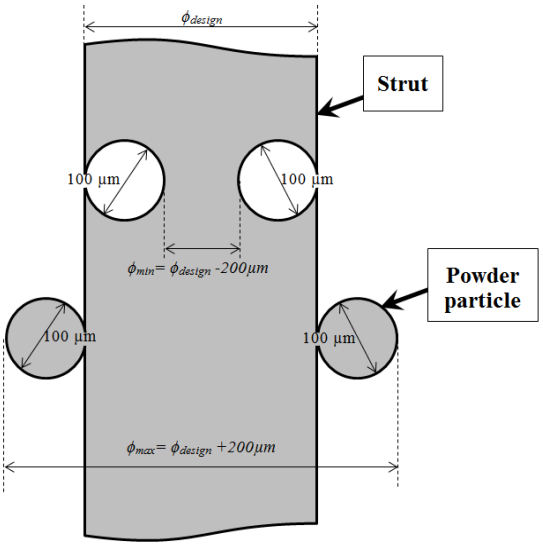

Fig. 3 Schematization of the strut diameter variation

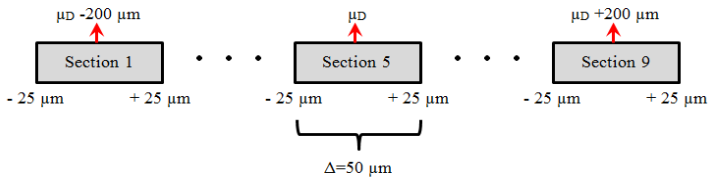

Fig. 4 Conversion of diameter value to section number

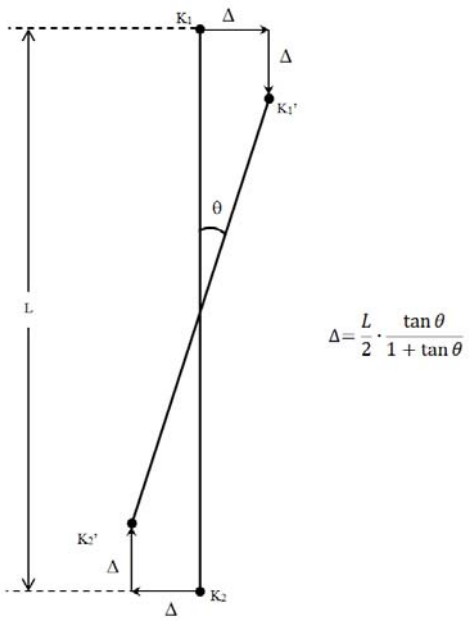

Fig. 5 Conversion of the inclination angle θ to keypoint shifting distance

Strut inclination

First each strut was approximated by a straight line. Then, the strut inclination angle (*Sinc*) was measured between this line and the coordinate axes for each non-fractured strut. Each sample face consists of 10 pores thus 11 struts in each direction, making at most 220 measures per face and 1320 for the entire sample. Measures were repeated twice and statistical analyses were performed to verify the repeatability of the measure (T-Student).

For the FE simulations, the extreme keypoints of each line K_1, K_2, K_1', K_2' were shifted a random distance (Δ), issued from a normal distribution. For this purpose, the measured minimum, mean, maximum, and standard deviation inclination angles (θ) were converted to the corresponding Δ as shown in Fig. 5. The same Δ was assumed in each direction, for a given inclination angle.

Fractured struts

The number of fractured struts (*Sfr*) was manually counted for each of the 6 faces of the non-tested S450P700 sample. The percentage of fractured struts (%*Sfr*) was obtained dividing the count of fractured struts by the total number of struts (220 for each face). In the FE model, each strut was randomly assigned a value between 0 and 1, issued from a uniform distribution. Struts assigned with a number larger than the percentage of fractured struts (%*Sfr*) were eliminated.

2.2.2 Finite element analyses

The 8 FE models of the sample S450P700 were simulated in ANSYS and the force-displacement curve was obtained. Then, the σ_{ap}-ε curve was computed by dividing the force and displacement by the apparent area and length of the samples, respectively. The E_{ap} was computed as the slope of the linear zone of the σ_{ap}-ε curve, and the $S_{Y,ap}$ by a parallel line at 0.2% strain. Due

Table 2 Measured strut inclination (*Sinc*) and fractured struts (*Sfr*) manufacturing irregularities of non-tested sample S450P700

		Mean (μ)	Standard deviation	Minimum value	Maximum value
Strut inclination	*Sinc* (◦)	0.05	8.28	-24.93	28.12
Fractured struts	*Sfr* (%)			13	

to their random nature, each model including manufacturing irregularities was simulated 5 times and results were averaged. FE results were compared with the experimental data in terms of E_{ap} and $S_{Y,ap}$. The model that yielded the closest results to experimental data was applied to the other two sample sets (S450P600 and S450P800) comparing the results with experimental data.

3. Results

3.1 Characterization of manufacturing irregularities

Table 2 presents the strut inclination (*Sinc*) and fractured struts (*Sfr*) manufacturing irregularities measured on the sample S450P700. One face was discarded from the results due to the high irregularities present, thus 5 of the 6 faces of the non-tested sample were used for the characterization. Values correspond to the average of 5 faces.

For *Sinc*, no statistical significant difference was found between the two measurements, indicating the repeatability of the measures.

As what concerns the strut diameter variation (*Dvar*), the mean value, as measured by Petrović *et al.* (2012), is shown in Table 1. Then, as explained in section 2.2.1, a maximum *Dvar* of ±200 μm was considered, and a standard deviation of 75 μm was used for the normal distribution.

3.2 Finite element analyses

First, results corresponding to the simulation of the idealized model and the 7 models including manufacturing irregularities are presented and compared with experimental data, for the sample S450P700. Then, the model that yielded the closest results to experimental data was used to analyze the other two sample sets (S450P600 and S450P800).

3.2.1 Influence of the three geometrical irregularities for set S450P700

Fig. 6 shows, for set S450P700, the stress-strain (σ_{ap}-ε) curves corresponding to the simulations of the idealized model (from n=1 simulation), the 7 models including the manufacturing irregularities (average curves from n=5 simulations) and the experimental tests (average curve from n=5 tests). The experimental σ_{ap}-ε curve (thick black, without markers) shows an initial concave zone (between ε=0 and ε≈0.03), followed by an apparently linear zone, and then a progressive transition to a lower slope zone (for ε≈0.08). The idealized FE model (thin, stripped black without markers) behavior is very different, with larger stress values and a marked transition from the linear elastic to the linear plastic zone (for ε≈0.01).

Including *Dvar* (dark blue with "○" markers) or *Sfr* (red with "×" markers) irregularities

separately, result in similar curves to the idealized model, with lower stress values (especially for *Sfr*) and less drastic elastic to plastic transition. However, the *Sinc* irregularity (green with "+" markers) produces a drastic change of the σ_{ap}-ε curve which becomes more similar to the experimental curve: an initial concave zone (from ε=0 to ε≈0.015) followed by an approximately linear zone and a progressive transition to a zone with lower slope (for ε≈0.04). Therefore, *Sinc* is the most influent irregularity.

When *Dvar* is combined either with *Sfr* (violet with "⊗" markers) or with *Sinc* (turquoise with "⊕" markers), curves are similar to those obtained considering only *Sfr* or *Sinc*, respectively. Therefore, *Dvar* is the less influent irregularity.

The combination of *Sfr* with *Sinc* (yellow with "✳" markers) or the three manufacturing irregularities (grey "⊛" markers) yield the closest results to the experimental data.

Fig. 7 presents, for set S450P700, the apparent elastic modulus (E_{ap}, hatched bars) and yield strength ($S_{Y,ap}$, plain bars), corresponding to the simulations considering the idealized model (n=1), the 7 models including manufacturing irregularities (n=5) and the experimental tests (n=5). The standard deviation is plotted as error bars. Values corresponding to $S_{Y,ap}$ are indicated in MPa while those corresponding to E_{ap} are in GPa.

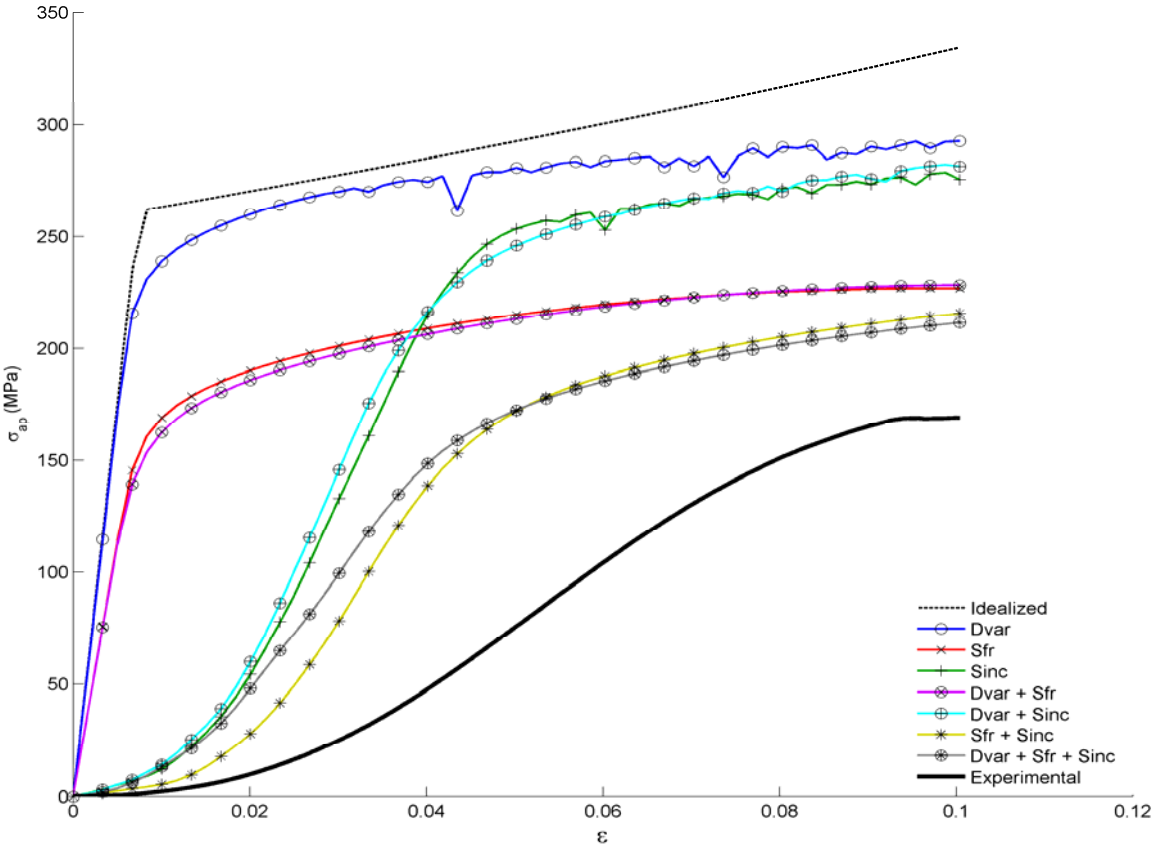

Fig. 6 Apparent stress-compressive strain (σ_{ap}-ε) curves for the set S450P700 obtained with the idealized model, the different combinations of manufacturing irregularities, and the experimental tests. *Dvar*: diameter variation; *Sfr*: fractured struts; *Sinc*: inclined struts; Exp: experimental

The computed $S_{Y,ap}$ using the idealized model (263 MPa) is almost twice the experimental measures (146±2.48 MPa). When considering *Dvar* ($S_{Y,ap}$=234±2.07 MPa) or *Sinc* ($S_{Y,ap}$=242±1.82 MPa) separately, similar but smaller $S_{Y,ap}$ values than the idealized model are obtained. When *Sfr* is considered alone, a large reduction in $S_{Y,ap}$ (166±8.22 MPa) is obtained and results are closer to experimental data. When *Dvar* and *Sinc* are combined, the $S_{Y,ap}$ (217±4.23 MPa) is similar and smaller than when *Dvar* or *Sinc* is considered alone. When *Sfr* is combined with any other manufacturing irregularity, $S_{Y,ap}$ is smaller but close to considering only *Sfr*, therefore this irregularity shows the strongest effect on $S_{Y,ap}$. The combination of the three manufacturing irregularities ($S_{Y,ap}$=157±7.29 MPa) yields the closest results to the experimental data.

Statistical tests (one-factor ANOVA) revealed that the $S_{Y,ap}$ differences between the four models including *Sfr* were not statistically significant at a significance level of 0.05 (i.e., the four models can be considered as equivalents for the $S_{Y,ap}$).

The computed E_{ap} using the idealized model (35.16 GPa) is more than 10 times larger than the experimental observations (2.82±0.21 GPa). Considering *Dvar* (E_{ap}=33.03±0.17 GPa) or *Sfr* (E_{ap}=22.1±1.07 GPa) separately reduces E_{ap}, but values remain one order of magnitude larger

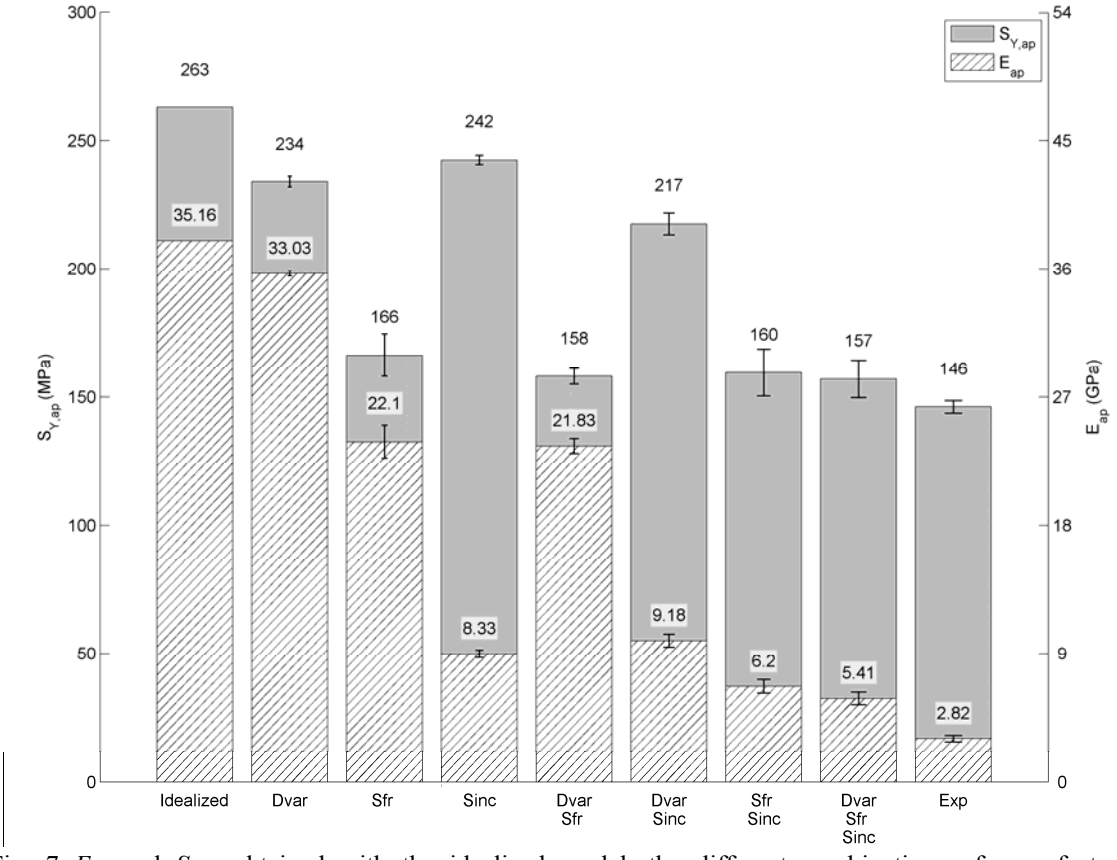

Fig. 7 E_{ap} and $S_{Y,ap}$ obtained with the idealized model, the different combinations of manufacturing irregularities, and the experimental tests for the set S450P700. *Dvar*: diameter variation; *Sfr*: fractured struts; *Sinc*: inclined struts; Exp: experimental

than experimental data. When *Sinc* is considered alone, computed E_{ap} (8.33±0.25 GPa) is of the same order of magnitude than the experimental measurements. When *Dvar* and *Sinc* (E_{ap}=9.18±0.42 GPa) are combined, slightly larger E_{ap} values than considering *Sinc* alone are predicted. When *Dvar* and *Sfr* are combined (E_{ap}=21.83±0.48 GPa), E_{ap} is close to when *Sfr* is considered alone. When *Sinc* is combined with other manufacturing irregularities, results are smaller and always close to considering *Sinc* alone, therefore this irregularity shows the strongest effect on E_{ap}. The best results are also obtained when the three manufacturing irregularities are combined (E_{ap}=5.41±0.41 GPa).

Statistical tests (T-Student) revealed that the differences between all models are statistically significant except for the *Sfr* ($E_{ap,comp}$=22.1±1.07 GPa) and *Dvar* combined with *Sfr* (E_{ap}=21.83±0.48 GPa), which can be assumed to produce equivalent results in terms of E_{ap}.

3.2.2 Simulation of the other sample sets

The methodology developed to include the three manufacturing irregularities (*Dvar*, *Sfr* and *Sinc*) was applied to the other two sample sets (S450P600 and S450P800). The *Sinc* and *Sfr* values

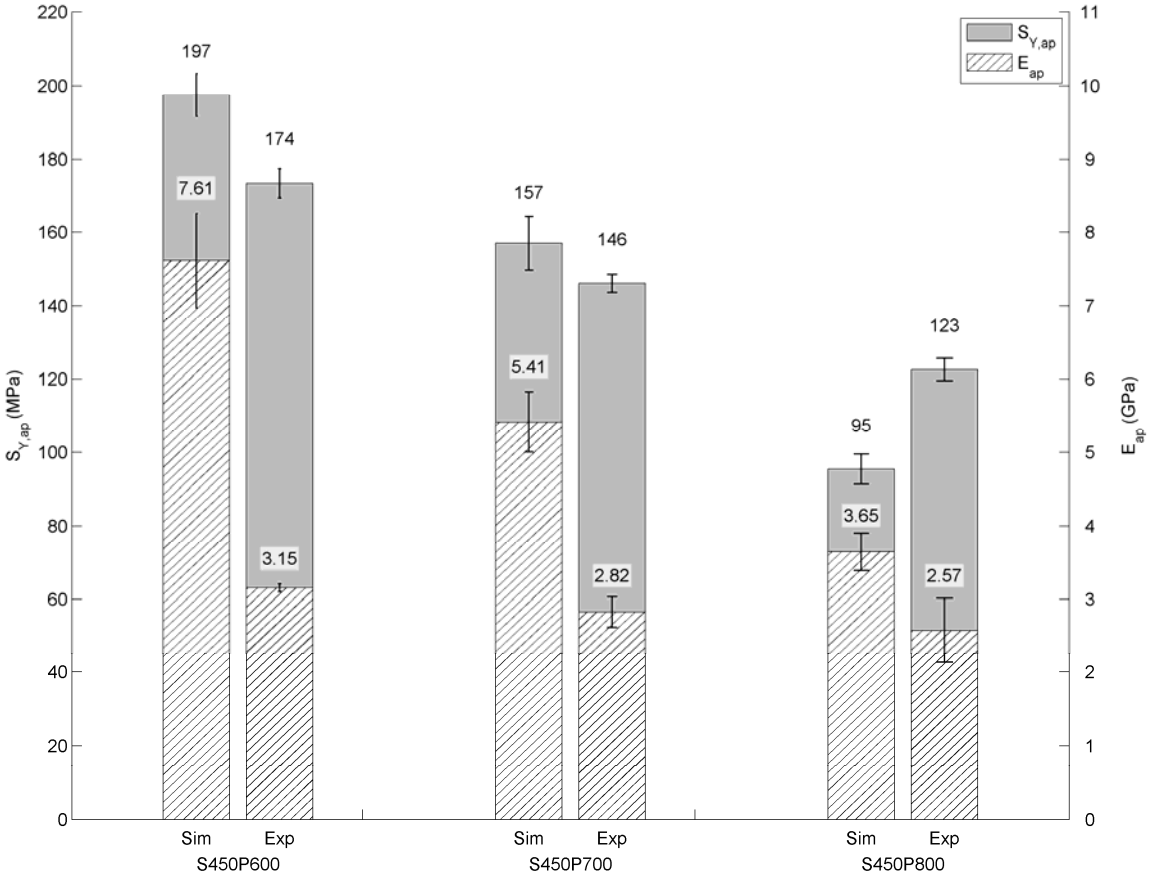

Fig. 8 Comparison of $S_{Y,ap}$ (plain bars) and E_{ap} (hatched bars) obtained from experimental tests (Exp) and from FE simulations including the three manufacturing irregularities (Sim) for the three sets (S450P600, S450P700 and S450P800)

were assumed to be the same as for the measured sample (S450P700). The strut and pore diameter values were taken from Petrović *et al.* (2012) and are shown in Table 1.

Fig. 8 shows, for the three sample sets, the comparison of $S_{Y,ap}$ (plain bars) and E_{ap} (hatched bars) computed with the FE model (marked as "Sim") and the experimental values (marked as "Exp"). The standard deviation is plotted as error bars. Values corresponding to $S_{Y,ap}$ are indicated in MPa while those corresponding to the E_{ap} are in GPa.

$S_{Y,ap}$ computed numerically is larger than experimental data for the sets S450P600 (197±5.82 MPa and 174±3.97 MPa, respectively) and S450P700 (157±7.29 MPa and 146±2.48 MPa, respectively). However for set S450P800 (i.e., the largest porosity), larger $S_{Y,ap}$ values were obtained experimentally (123±3.06 MPa) than computationally (95±4.09 MPa). Maximum difference is obtained for set S450P800 and minimum difference for set S450P700, which is the sample used for the characterization of irregularities.

Regarding E_{ap}, although the numerical values obtained are larger, they are of the same order of magnitude than experimental values for all three sets. Set S450P600 (i.e., smallest porosity) shows the maximum difference between computed (7.61±0.64 GPa) and experimental E_{ap} (3.15±0.05 GPa). Set S450P800 (largest porosity) shows the minimum difference between computed (3.65±0.26 GPa) and experimental E_{ap} (2.57±0.44 GPa).

4. Discussion

In the present study, three manufacturing irregularities obtained from direct observations (strut inclination, strut diameter variation and fractured strut) were characterized on an EBM-produced sample of well-ordered porous metallic material. An idealized model and models including different combinations of these manufacturing irregularities were simulated using FE models. The results were compared with experimental data in terms of the apparent stress-strain curve (σ_{ap}-ε), the apparent elastic modulus (E_{ap}) and the apparent yield strength ($S_{Y,ap}$).

For the sample S450P700 (strut diameter of 450 μm and pore diameter of 700 μm), including the three manufacturing irregularities in the FE models resulted in a predicted σ_{ap}-ε curve similar to the experimental one. In addition, the E_{ap} was reduced compared to an idealized model from 35.16 GPa to 5.41±0.41 GPa which is a value close to the experimental one of 2.82±0.21 GPa. The same was observed for the $S_{Y,ap}$, which decreased from 263 MPa to 157±7.29 MPa, much closer to the experimental value of 146±2.48 MPa. The combination of the three manufacturing irregularities also produced close results to the experimental values when applied to the other sets (S450P600 and S450P800), confirming the applicability of the developed model for the range of strut and pore sizes tested.

These results are in accordance with previous works considering manufacturing irregularities: (Campoli *et al.* 2013), (Hazlehurst *et al.* 2013) who found a reduction of E_{ap} from 16.03 to 5.37 GPa; and (Karamooz Ravari and Kadkhodaei 2015), who found an E_{ap} that was around 91% of the experimental one. However, in this last case the chosen unit-cell (BCC) already showed a small difference between numerical and experimental results (around 15%) without considering manufacturing irregularities (Smith *et al.* 2013).

The strut inclination (*Sinc*) was the most influent manufacturing irregularity on the computed σ_{ap}-ε curve and on E_{ap}. This is in accordance with Luxner *et al.* (2009), Alkhader and Vural (2008), and with (Ashby 2006) who observed a 10 times difference in E_{ap} between stretch and bending dominated porous materials. Perfectly aligned struts carry the load axially, however for inclined

struts the load is no longer aligned with their axis, which induces bending of the struts (Luxner *et al*. 2007) and consequently reduces the overall stiffness and strength (Alkhader and Vural 2008).

The fractured struts (*Sfr*) was the most determinant manufacturing irregularity influencing $S_{Y,ap}$. This is in accordance with Chen *et al.* (1999). When fractured struts are present, their load is distributed between the surrounding struts which become more solicited thus yielding earlier.

Additional investigation is needed to understand why the numerically computed $S_{Y,ap}$ for set S450P800 is smaller than the experimental one. It is not clear whether it is due to the larger pore size (i.e., more slender struts) for which bending effects are more important; or to the difference in the measured strut diameter compared to the two other sets. As shown in Table 1, sets S450P600 and S450P700 have similar strut diameters: 648 and 666 μm, respectively; however set S450P800 shows considerably smaller strut diameter, almost 100 μm smaller (577 μm). Also, additional studies are required to assess the performance of the proposed model under different loading conditions, such as bending and torsion.

In the present work we showed that not taking into account the manufacturing irregularities in the FE models lead to an overestimation of the mechanical properties of well-ordered porous materials. This may negatively impact the design of implants made with porous materials (Parthasarathy *et al.* 2011, Xiao *et al.* 2013). The proposed methodology is a simple way to measure and simulate manufacturing irregularities from a physical sample and this is precisely its strength. The results of the present study show that good agreement between numerical and experimental results can be obtained with little characterization and modeling effort. However, this study showed some limitations. First only one sample was used for the characterization of manufacturing irregularities, which were assumed to be similar for the other samples and were measured on exterior faces. Second, little data corresponding to the strut diameter variation was available and the standard deviation of the diameter was assumed to be 75 μm based on geometrical considerations. Third, although statistical tests showed no influence, hand measures may be subjective since measured twice by the same person.

5. Conclusions

In this study, a simple methodology to characterize and include the most noticeable manufacturing irregularities in the FE models of well-ordered porous materials was presented.

- Manufacturing irregularities may explain the lack of agreement between experimental data and numerical simulations.
- The inclination of struts plays a critical role in the outcomes of the apparent elastic modulus.
- The fractured struts play a critical role in the outcomes of the apparent yield strength.
- We recommend including strut diameter variation, inclined struts and fractured struts in the FE models in order to better predict the mechanical behavior of well-ordered porous materials for implant applications.

Acknowledgments

Authors would like to acknowledge the Biomechanic's Institute of Valencia (Spain) for the precious experimental data that made possible this study. This study was supported by the Individual Discovery Grant Program from the Natural Sciences and Engineering Research Council

of Canada (NSERC).

References

Adjari, A., Nayeb-Hashemi, H., Canavan, P. and Warner, G. (2008), "Effect of defects on elastic-plastic behavior of cellular materials", *Mater. Sci. Eng., A*, **487**(1), 558-567.

Ahmadi, S.M., Campoli, G., Amin Yavari, S., Sajadi, B., Wauthle, R., Schrooten, J., Weinans, H. and Zadpoor, A.A. (2014), "Mechanical behavior of open-cell porous biomaterials made of diamond lattice unit cells", *J. Mech. Behav. Biomed. Mater.*, **34**, 106-115.

Alkhader, M. and Vural, M. (2008), "Mechanical response of cellular solids: Role of cellular topology and microstructural irregularity", *Int. J. Eng. Sci.*, **46**(10), 1035-1051.

Arabnejad, S. and Pasini, D. (2012), "Multiscale design and multiobjective optimization of orthopedic hip implants with functionally graded cellular material", *J. Biomech. Eng.*, **134**(3), 031004-1-031004-10.

Arabnejad, S. and Pasini, D. (2013), "Mechanical properties of lattice materials via asymptotic homogenization and comparison with alternative homogenization methods", *Int. J. Mech. Sci.*, **77**, 249-262.

ARCAM AB. Ti6Al4V ELI Titanium Alloy. From http://www.arcam.com/wp-content/uploads/Arcam-Ti6Al4V-ELI-Titanium-Alloy.pdf

Ashby, M.F. (2006), "The properties of foams and lattices", *Philos. Trans. R. Soc. Lonodon, Ser. A*, **364**(1838), 15-30.

Barbas, Q., Bonnet, A.-S., Lipinski, P., Pesci, R. and Dubois, G. (2012), "Development and mechanical characterization of porous titanium bone substitutes", *J. Mech. Behav. Biomed. Mater.*, **9**, 34-44.

Campoli, G., Borleffs, M.S., Amin Yavari, S., Wauthle, R., Weinans, H. and Zadpoor, A.A. (2013), "Mechanical properties of open-cell metallic biomaterials manufactured using additive manufacturing", *Mater. Des.*, **49**, 957-965.

Chen, C., Lu, T.J. and Fleck, N.A. (1999), "Effect of imperfections on the yielding of two-dimensional foams", *J. Mech. Phys. Solid.*, **47**(11), 2235-2272.

Fraldi, M., Esposito, L., Perrella, G., Cutolo, A. and Cowin, S.C. (2010), "Topological optimization in hip prosthesis design", *Biomech. Model. Mechanobiol.*, **9**(4), 389-402.

Harrigan, J., Reida, S. and Yaghoubib, S. (2010), "The correct analysis of shocks in a cellular material", *Int. J. Impact Eng.*, **37**(8), 918-927.

Hazlehurst, K., Wang, C.J. and Stanford, M. (2013), "Evaluation of the stiffness characteristics of square pore CoCrMo cellular structures manufactured using laser melting technology for potential orthopaedic applications", *Mater. Des.*, **51**, 949-955.

Heo, H., Ju, J. and Kim, D.-M. (2013), "Compliant cellular structures: Application to a passive morphing airfoil", *Compos. Struct.*, **106**, 560-569.

Herrera, A., Yánez, A., Martel, O., Afonso, H. and Monopoli, D. (2014), "Computational study and experimental validation of porous structures fabricated by electron beam melting: A challenge to avoid stress shielding", *Mater. Sci. Eng., C*, **45**, 89-93.

Karamooz Ravari, M.R. and Kadkhodaei, M. (2015), "A computationally efficient modeling approach for predicting mechanical behavior of cellular lattice structures", *J. Mater. Eng. Perform.*, **24**(1), 245-252.

Kuiper, J.H. and Huiskes, R. (1997), "Mathematical optimization of elastic properties: application to cementless hip stem design", *J. Biomech. Eng.*, **119**(2), 166-174.

Kumar, V., Manogharan, G. and Cormier, D.R. (2009), "Design of periodic cellular structures for heat exchanger applications", *20th Solid Freeform Fabrication Symposium*, Texas, August, 738-748.

Luxner, M.H., Stampfl, J. and Pettermann, H. (2007), "Numerical simulations of 3D open cell structures-Influence of structural irregularities on elastoplasticity and deformation localization", *Int. J. Solids Struct.*, **44**(9), 2990-3003.

Luxner, M.H., Stampfl, J. and Pettermann, H.E. (2005), "Finite element modeling concepts and linear

analyses of 3D regular open cell structures", *Mech. Behav. Cell. Solid.*, **40**(22), 5859-5866.
Luxner, M.H., Stampfl, J. and Pettermann, H.E. (2009), "Nonlinear simulations on the interaction of disorders and defects in open cell structures", *Comput. Mater. Sci.*, **47**(2), 418-428.
Maloney, K.J., Fink, K.D., Schaedler, T.A., Kolodziejska, J.A., Jacobsen, A.J. and Roper, C.S. (2012), "Multifunctional heat exchangers derived from three-dimensional micro-lattice structures", *Int. J. Heat Mass Transfer.*, **55**(9-10), 2486-2493.
Parthasarathy, J., Starly, B. and Raman, S. (2011), "A design for the additive manufacture of functionally graded porous structures with tailored mechanical properties for biomedical applications", *J. Manuf. Processes*, **13**(2), 160-170.
Petrović, V., Blasco, J.R., Portolés, L., Morales, I., Primo, V., Atienza, C., Moreno, J.F. and Belloch, V. (2012), *A study of mechanical and biological behavior of porous Ti6Al4V fabricated on EBM*, *Innovative Developments in Virtual and Physical Prototyping*, Taylor and Francis, London, United Kingdom, 115-120.
Quevedo González, F.J. and Nuño, N. (2015), "Finite element modelling approaches for well-ordered porous metallic materials for orthopaedic applications: cost effectiveness and geometrical considerations", *Comput. Meth. Biomech. Biomed. Eng*., 1-10.
Smith, M., Guan, Z. and Cantwell, W.J. (2013), "Finite element modelling of the compressive response of lattice structures manufactured using the selective laser melting technique", *Int. J. Mech. Sci.*, **67**, 28-41.
Spadoni, A. and Ruzzene, M. (2007), "Static aeroelastic response of chiral-core airfoils", *J. Intell. Mater. Syst. Struct.*, **18**, 1067-1075.
Xiao, D., Yang, Y., Su, X., Wang, D. and Sun, J. (2013), "An integrated approach of topology optimized design and selective laser melting process for titanium implants materials", *Bio-Medical Mater. Eng.*, **23**(5), 433-445.
Zhu, H.X., Hobdell, J.R. and Windle, A.H. (2001), "Effects of cell irregularity on the elastic properties of 2D Voronoi honeycombs", *J. Mech. Phys. Solids.*, **49**(4), 857-870.

MC